Investigation of Linear Magnetic Anomalies in the Funeral Mountains, Death Valley Region, California

By John W. Hillhouse and Robert Morin[1]

Open-File Report 03-12

2004

U.S. DEPARTMENT OF THE INTERIOR
U.S. GEOLOGICAL SURVEY

[1]Menlo Park, Calif.

ABSTRACT

A series of northeast-trending magnetic anomalies were detected in the Funeral Mountains with a high-resolution aeromagnetic survey of the Death Valley-Amargosa Desert region of California and Nevada. We report results of a ground-level magnetic survey that ties the anomalies to strongly magnetic beds within the Stirling Quartzite. The study area covers 18 km^2 near Indian Pass, approximately 30 km south of Beatty, Nevada. Member A of the Stirling Quartzite contains magnetite-rich schist, characterized by magnetic susceptibility of 0.015 (SI). The magnetic beds, which are concentrated in a 37-m thick interval, crop out in three ridges separated by sub-parallel normal faults. Two-dimensional modeling of the magnetic profile over one of the ridges fits an east-dipping layer, consistent with the local geologic structure. In the Death Valley region, spring alignments and magnetic anomalies appear to be related. Although we found no evidence in the Funeral Mountains that the fault zones are unusually magnetic, the normal faults produce lengthy tilted blocks that do produce magnetic anomalies from upturned magnetic beds within the blocks. In this way, patterns of spring occurrence and linear aeromagnetic anomalies may both reflect the regional geologic structure.

INTRODUCTION

From analysis of high-resolution aeromagnetic data, Blakely and others (2000) discovered subtle magnetic lineations that mark buried geologic structures in the Amargosa Desert and Death Valley region of California and Nevada. Their studies suggest that many of the linear magnetic anomalies overlie faults that produce ridges in basement rocks. An intriguing observation is the coincidence of magnetic anomalies with water-spring alignments, many of which occur in alluvial aprons flanking mountains. Blakely and others (2000) offered the hypothesis that spring locations are largely controlled by faults in basement rocks concealed by alluvium, and the magnetic anomalies are expressions of fracture zones that serve as groundwater conduits.

A puzzling aspect of the Death Valley magnetic studies is the occurrence of linear magnetic anomalies in presumably nonmagnetic basement terrain in the Funeral Mountains. There, metasedimentary rocks such as the Stirling Quartzite are dominant. Several subparallel positive magnetic features extend southward across the northern Funeral Mountains and terminate in alluvium flanking Death Valley (Figure 1). The magnetic anomalies trend toward a cluster of springs that are major water sources for the National Park. After noting the apparent alignment of springs, faults, and magnetic features in the Funeral Mountains, Blakely and others (2000) proposed that groundwater might be following the pattern of faults. But it remained a mystery as to why faults in quartzites, which are expected to be weakly magnetized, would produce features that could be detected in an aeromagnetic survey.

The objective of the current study was to determine the source of linear magnetic anomalies in the Funeral Mountains via a ground magnetic survey. The area of our survey comprises approximately 18 km^2 in the southwest corner of the Ashton 7 ½ ‘ topographic quadrangle and the southeast corner of the East of Chloride Cliff quadrangle (Figure 2). Reduction of

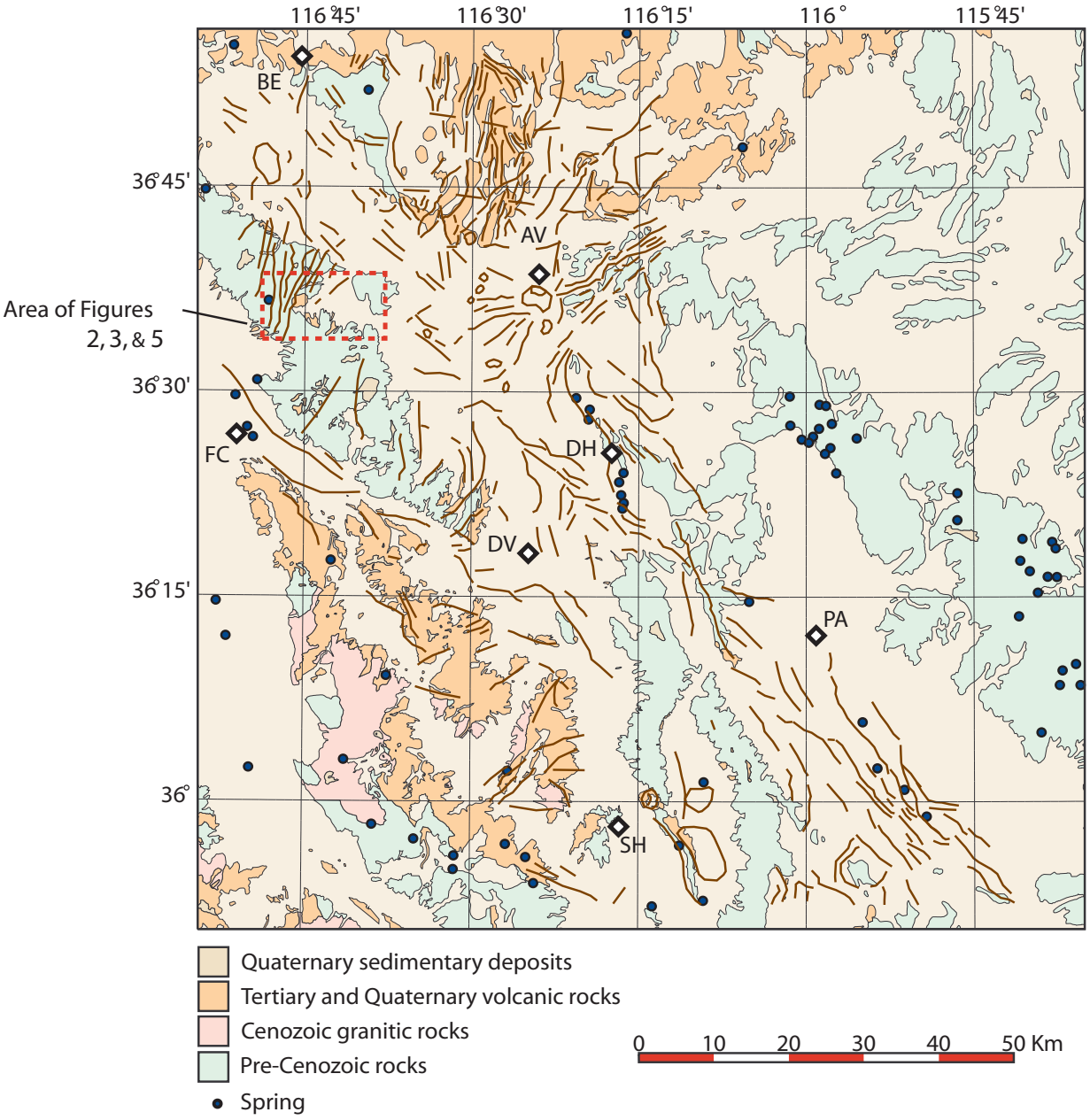

Figure 1. Simplified geologic map of the eastern Death Valley Region, California and Nevada, showing magnetic lineations derived from the aeromagnetic survey. AV, Amargosa Valley; BE, Beatty; DH, Devils Hole; DV, Death Valley Junction; FC, Furnace Creek; PA, Pahrump; SH, Shoshone. Figure adapted from Blakely and others (2000); geology adapted from Jennings (1977) and Stewart and Carlson (1978).

the aeromagnetic data to enhance shallow-sourced, small wavelength features revealed five subparallel linear anomalies in the survey area (Figure 3). These are the same anomalies that extend southward toward the springs near Furnace Creek. At the elevation of the airborne survey (150 m), the peak anomaly amplitudes are about 2 nT above the filtered base level. In March and May, 2001, we conducted a ground survey of the area using a continuously recording magnetometer and GPS locater. The ground traverses crossed three linear anomalies that had been revealed by analysis of the previous aeromagnetic survey. During the traverses, magnetic susceptibilities of outcrops were spot checked with a hand-held meter. Here we present the results of the ground magnetic survey and discuss the source of linear magnetic anomalies in the Funeral Mountains.

GEOLOGY

Access to the study area is via an unimproved road that leaves Highway 95 at the junction of Steves Pass road, about 13 miles south of Beatty, Nevada. According to mapping by Wright and Troxel (1989a), the survey area is primarily underlain by Stirling Quartzite of late Proterozoic age (Figure 2). The Stirling Quartzite is divided into five members comprising fine to coarse-grained sandstone, siltstone, and thin-bedded carbonate rocks. Wright and Troxel (1989a) described the sequence in stratigraphic order as: "Member A, mostly fine- to coarse-grained sandstone, ranging from orthoquartzite to arkose; contains abundant beds of quartz-pebble conglomerate and platy siltstone. Also contains a dolomite and limestone marker bed in upper part…"; "Member B: Fine-grained arkosic sandstone, micaceous siltstone, and beds of carbonate rocks; typically laminated. Siltstone within this member metamorphosed to garnet-bearing schist in northern Funeral Mountains."; "Member C: Dolomite and limestone; massive to thin-bedded and very fine grained, upper part silty in northern part…"; "Member D: Mostly fine- to medium-grained feldspathic sandstone; siltstone layers common in lower part and are progressively less abundant upward.", "Member E: Medium- to coarse-grained sandstone; mostly altered to orthoquartzite." The lower three members (A, B, and C) comprise nearly all of the bedrock exposures in our study area.

Member A of the Stirling Quartzite underlies a series of subparallel ridges and low hills that are mapped as northeast-trending fault blocks (Wright and Troxel, 1989a,b). Bedding within the blocks strikes northeast and dips moderately (30° - 60°) to the southeast. The blocks are bounded by normal faults that dip to the northwest. Normal displacements on the faults have created an aligned map pattern, which repeats exposures of the lower members in the study area. From a preliminary inspection of the enhanced aeromagnetic anomalies it was clear that the linear magnetic features were directly above the ridges composed of Member A, and that the linear features were roughly parallel to the strike of sedimentary bedding and trend of normal faults noted above.

SURVEYING METHODS

Most magnetic surveys employ a single sensor that measures total intensity of the ambient magnetic field. Each measurement is dominated by the magnetic field that originates from Earth's molten core. This field varies smoothly due to the great depth of the source. Small perturbations relative to the core field are produced by magnetic sources in the underlying rocks

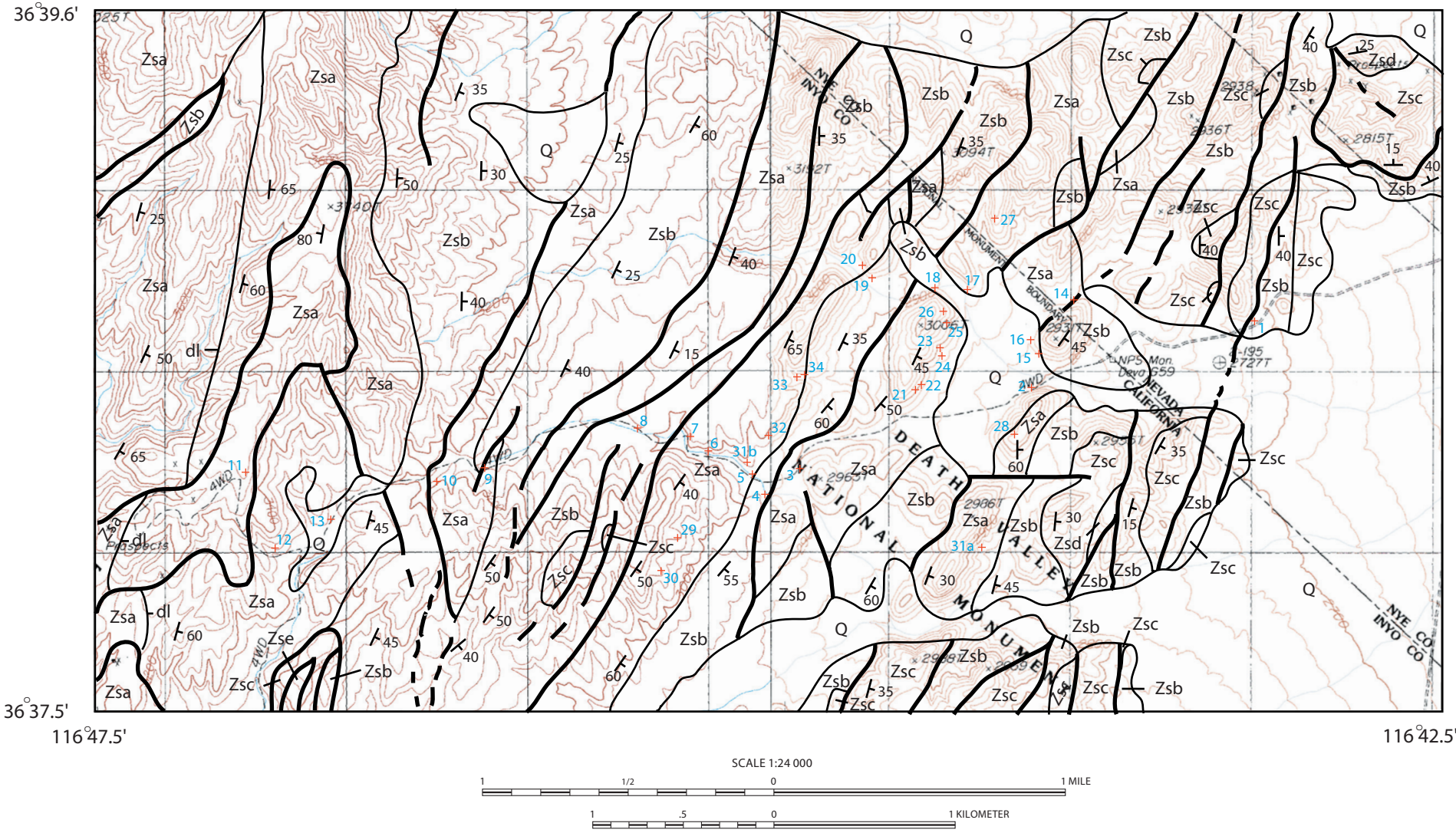

Figure 2. Geologic map of the detailed survey area. Faults (heavy lines) and depositional geologic contacts (fine solid lines) are from Wright and Troxel (1989a): Q, Quaternary alluvium; Zsa,…Zse, Stirling Quartzite Members A, B,C, D, and E; dl, dolomite and limestone bed within Member A in western area of map. Numbered sites (+) indicate locations of magnetic susceptibility measurements keyed to Table 1.

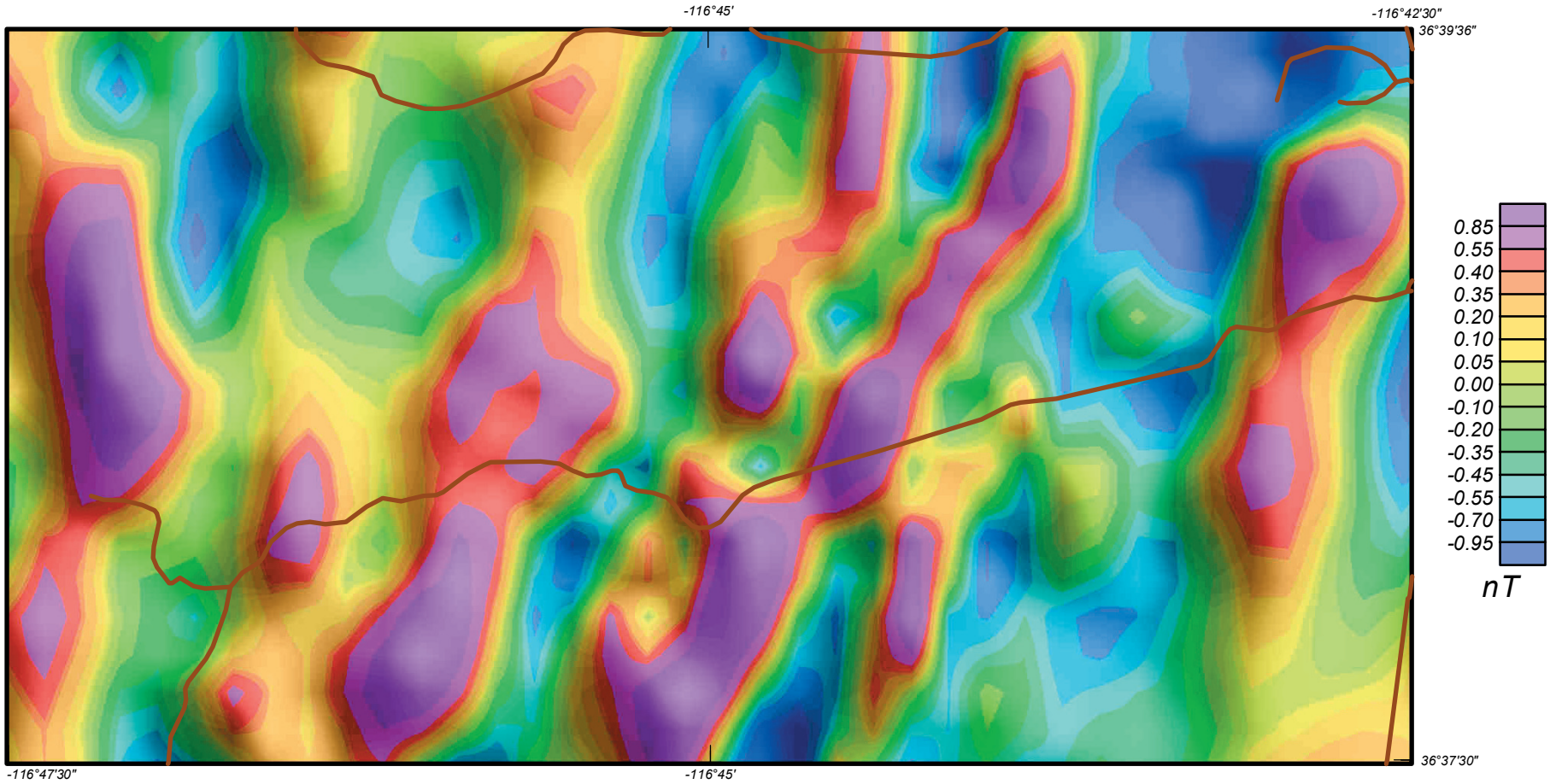

Figure 3. Aeromagnetic map of study area in the Funeral Mountains. To produce this map of residual magnetic anomalies, the original survey data were filtered to emphasize shallow-sourced features. Solid red lines denote roads.

and by solar magnetic fields. At the latitude and elevation of our study area, the core field strength is approximately 50,000 nT and the daily solar effect is about ±15 nT (In the SI unit system, magnetic field intensity is given in nanoTesla (nT). Subtracting the core field and solar effects from survey measurements emphasizes magnetic fields produced by rock bodies and structures near the earth's surface.

The magnetization (M) of a unit-volume of rock is given as the vector sum of the remanent magnetization (M_r) and the induced magnetization (kH), where k is the magnetic susceptibility and H is the ambient magnetic field; i.e., $M = M_r + kH$. In most cases, concentration of magnetite is the primary factor that determines the strengths of remanent and induced magnetizations. With the exception of volcanic rocks, which typically have very strong remanent magnetizations, most rock types produce magnetic anomalies through contrasts in induced magnetization.

A magnetic survey conducted at ground level is very sensitive to contrasts in magnetic properties at shallow depth. Therefore, a ground survey is ideal for locating thinly buried faults and bedding contacts. Extremely high magnetic gradients, as produced by lightning strikes at the ground surface, can produce inaccurate or misleading measurements in total-field sensors. To minimize these problems, it is desirable to carry the magnetometer several meters above the ground surface.

The instruments used in our ground survey consisted of a cesium-vapor magnetometer (Geometrics G-858) and a Trimble global-positioning-system (GPS) receiver carried in a backpack (Figure 4). As the operator walks over the terrain, the intensity of the magnetic field and the operator's position are recorded at regular intervals, one second in this study. The magnetic sensor was carried at a nominal height of 2.5 m above the ground surface. Horizontal positional accuracy of the GPS unit is assumed to be ± 1 m as stated by the manufacturer. At the beginning of each day's survey, we set up a base-station magnetometer (Geometrics G-856) to record diurnal geomagnetic variations at two-second intervals during the survey period. The first day of surveying (March 27, 2001) covered the jeep road and a wash north of the road (Figure 2). A battery failure halted the survey at the end of the first day, and we returned to complete the traverses during May 1-2, 2001. Using the aeromagnetic survey as a guide, we concentrated the ground traverses where linear magnetic anomalies had been noted. The sparse desert vegetation posed no barriers to our survey, but loose rock and the steep terrain posed challenges for the operators.

The roving magnetometer data were processed through standard Geometrics magnetic processing software, which corrected for the diurnal variation and added the location information from the GPS. Geometrics' technique for making the diurnal correction is to subtract the total-field magnetic base station measurements from the total-field rover measurements leaving a small anomalous value rather than a large total-field value. These data were then converted to a format compatible with in-house Fortran computer programs. To this file, GPS elevations were added. The accuracy of the vertical component of this GPS system is about ± two meters. GPS location data were collected on the WGS-84 (World Geodetic System 1984) horizontal datum. Location conversion was made between the WGS-84 horizontal datum and the NAD27 (North American Datum 1927) datum for correct correlation with topographic and geologic maps used for interpretation. These data were then plotted and inspected at traverse crossings. The magnetic data of the different traverses were shifted up or down to fit at the traverse crossings.

Magnetic susceptibility readings were made at selected outcrops by a second person following the magnetometer operator. The readings were made with a hand-held meter pressed against

the outcrop (Table 1). The meter reads out susceptibility in dimensionless SI units. At each location, several readings were taken across several meters of outcrop to represent the variation of rock types. Locations of the susceptibility readings were logged with a second GPS unit to a precision of ±0.001' in latitude and longitude (Figure 2).

Figure 4. Portable magnetometer/GPS instrument deployed in the field.

RESULTS

The ground survey revealed three prominent magnetic anomalies, as shown by the contoured magnetic map (Figure 5). Each anomaly is a narrow, elongate feature that trends northeast across the surveyed area. Peak-to-peak amplitudes of the anomaly crossings average approximately 400 nT. The magnetic variation (± 50 nT) over the intervening area is quite subdued relative to the prominent linear anomalies. Each of the three anomalies lies above a narrow interval near the top of Member A of the Stirling Quartzite. The axes of the anomalies closely follow the quartzite bedding and do not appear close to any of the normal faults.

We have selected magnetic records from several traverses across the middle anomaly for more detailed analysis and modeling (Figure 6). The zone of magnetic disturbance typically spans 100-200 m in a direction normal to the anomaly trend. In terms of form, each magnetic traverse shows a moderate rise on the southeast side, a sharp positive peak, and then a steep decline to negative values on the northwest side. Short wavelength features are commonly superimposed on the general form of the magnetic variation. The short features, which probably arise from localized magnetic variations spanning a few meters, do not correlate strongly from profile to profile.

Inspection of the susceptibility readings (Table 1) reveals a bimodal distribution of values. The majority have values of 10^{-5} -10^{-4} (SI) and typify readings from quartzites and limestones in the magnetically subdued areas. The second group has much higher values of susceptibility (5×10^{-3} to 5×10^{-2}), predominantly found in schists of Member A and associated with the linear magnetic anomalies.

MODELING

The consistent association of the linear magnetic anomalies with Member A of the Stirling Quartzite led to a simple 2D model that consisted of a thin dipping layer (Figure 7). The model assumes that the total anomaly is caused by induced magnetization from the ambient field (Inclination = 62º; declination = 14º east; intensity = 50,280 nT) acting on a thin layer dipping southeast. The model does not attempt to fit the short-wavelength features noted above. We used a susceptibility contrast of 0.015 (SI), in keeping with readings taken in the field. After several interations, a good fit between the modeled and observed magnetic anomaly was obtained from a 37-m-thick layer dipping 54º. This model is consistent with the geologic structure mapped in the vicinity of the middle anomaly. From visual inspection of all traverses across the linear magnetic anomalies, we conclude that a simple east-dipping layer in accord with the mapped geologic structure is the likely source of the anomalies. It is clear that the sedimentary bedding produces the magnetic anomaly; the northwest-dipping faults have no significant magnetic expression.

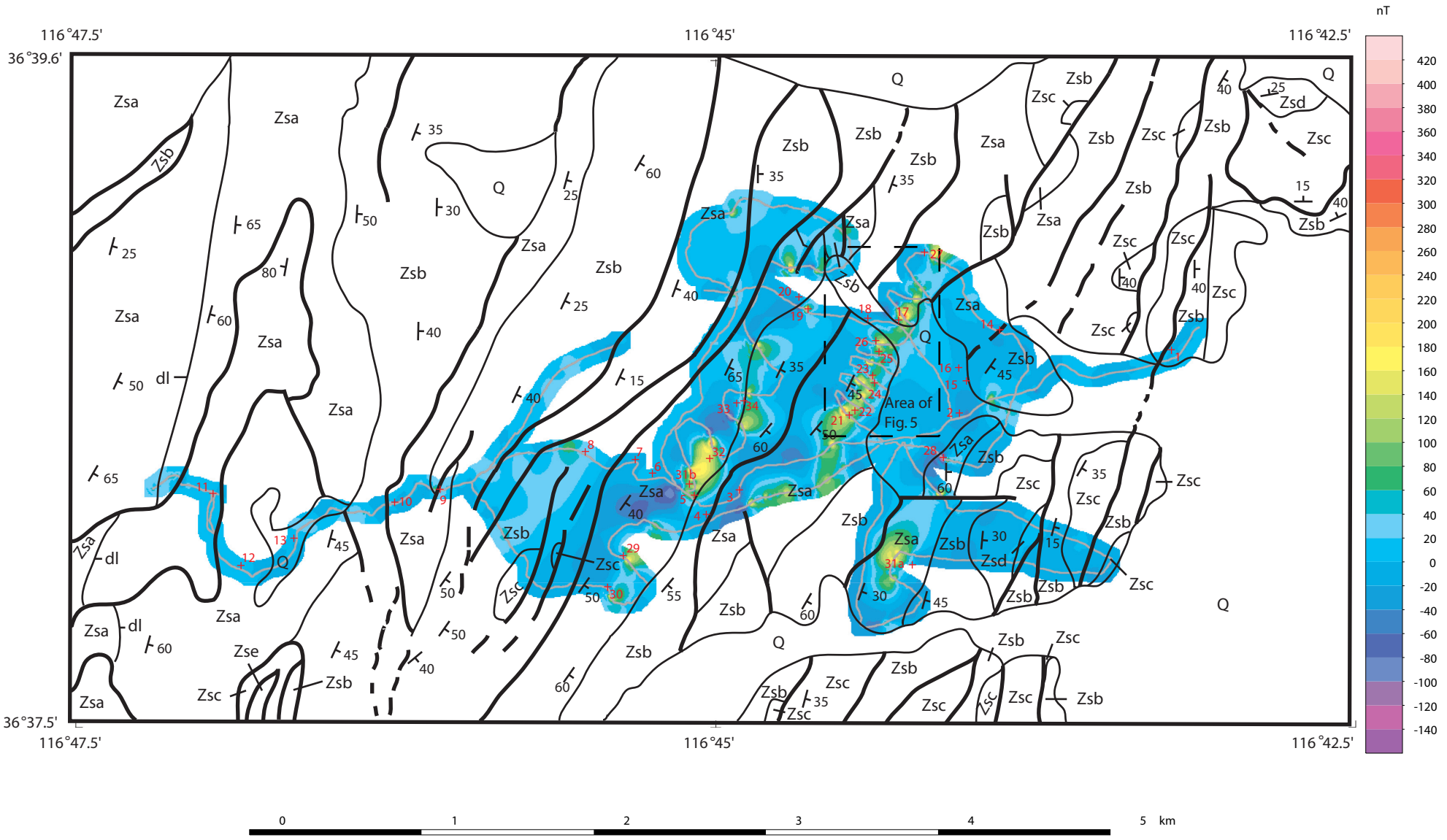

Figure 5. Colored areas denote magnetic anomalies inferred from the traverses (gray lines) of the ground survey. Geologic map and susceptibility measurement sites from Figure 2 are shown for reference. The stronger magnetic anomalies occur within Member A of the Stirling Quartzite. See Figure 2 for explanation of geologic symbols.

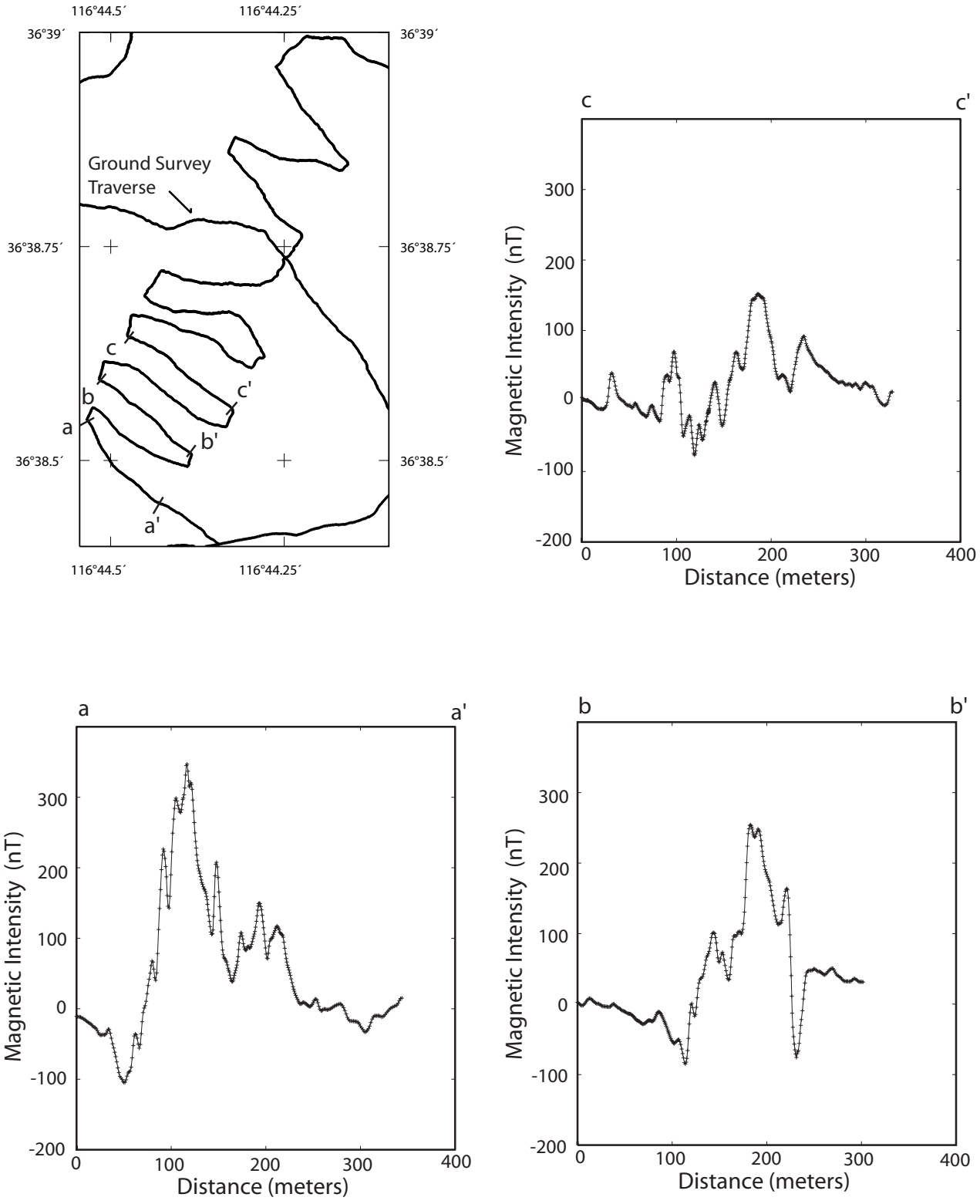

Figure 6. Magnetic profiles measured during three crossings of the middle magnetic feature shown in Figure 5.

DISCUSSION

The higher magnetic susceptibility readings occur in schist and fine-grained quartzites that contain relatively high concentrations of magnetite crystals. Under a hand lens, the magnetite grains stand out as euhedral crystals, typically 0.1 – 0.5 mm in diameter, against the very fine-grained matrix of the rock (Figure 8). The enriched magnetite zones appear to have formed by recrystallization of iron-bearing minerals during regional metamorphism. The magnetite crystals have concentrated in a restricted part of the stratigraphic section where chemical conditions were favorable for formation of magnetite. From the lithology, we infer that the recrystallization occurred at relatively high pressure and temperature, and was not the product of near-surface hydrothermal activity.

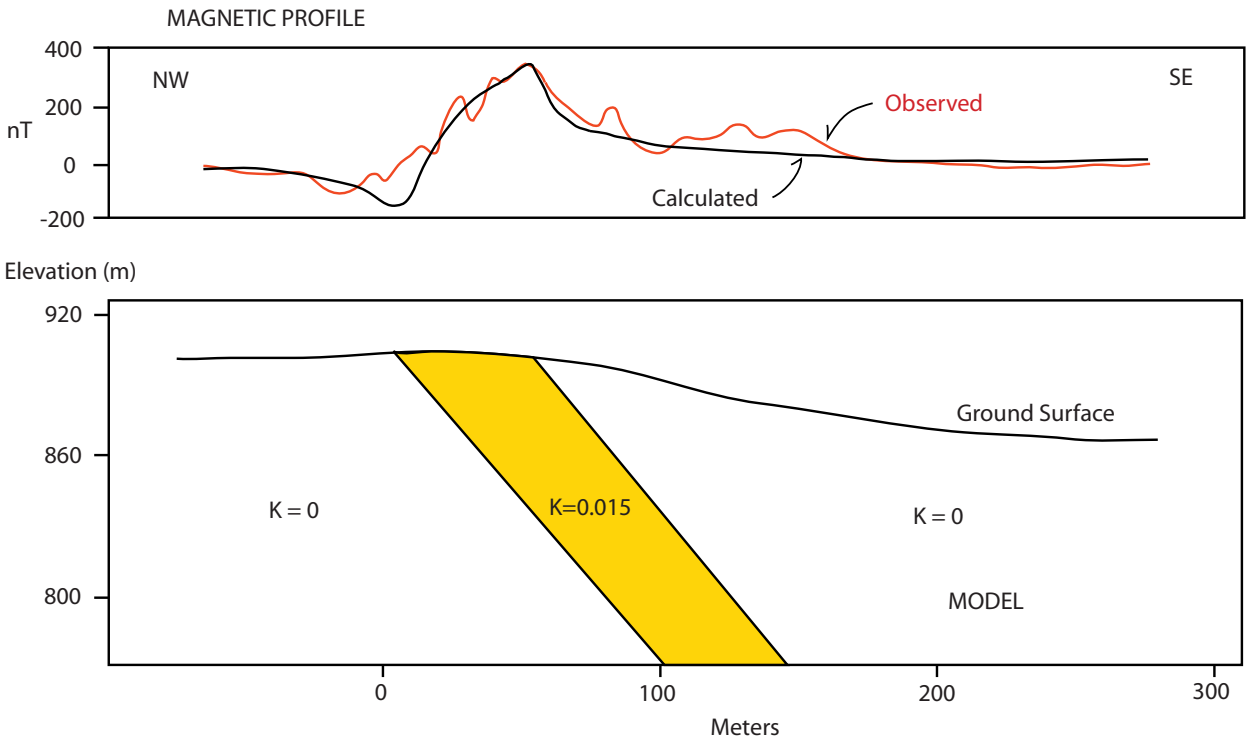

Figure 7. The calculated magnetic profile of a dipping layer is a good fit to the amplitude and smoothed form of the observed profile a-a' of Figure 6.

As would be expected, the higher magnetic susceptibility readings correspond closely with the strongly positive magnetic anomalies near the crest of the hill along the traverse of the middle anomaly. The dominant lithology at the hillcrest is schist, which is magnetite-rich and apparently resistant to erosion. The adjacent anomalies show similar correlations of high magnetic field, high susceptibility, stratigraphic position, and ridge-like topography. In each case, strongly magnetic zones occur in the upper part of Member A of the Stirling Quartzite approximately 20 meters below the contact with Member B.

Figure 8. Specimen (01SQ028, Table 1) of schist speckled with black magnetite crystals. The schist is from a bed within Member A of the Sterling Quartzite.

CONCLUSIONS

Our ground magnetic survey has verified the linear magnetic anomalies that were extracted from aeromagnetic data in the Funeral Mountains. Regional metamorphism created a strongly magnetic zone within the Stirling Quartzite. This zone is about 37 m thick and contains magnetite-rich schist that produces a susceptibility contrast of 0.015 (SI) relative to the magnetic properties of the surrounding strata. As indicated by the aeromagnetic map (Blakely and others, 2000), the strongly magnetic beds extend well beyond our ground-surveyed area both to the north and south. Because a strong correlation exists between Member A and the magnetic zone, it may be possible to refine the regional geologic map through magnetic mapping.

Although the Funeral Mountains magnetic anomalies trend toward Furnace Creek in Death Valley where the major springs are found, we found no close association of the actual magnetic source with faults, springs, or spring deposits. The anomaly-producing schists, that are quite dense and impermeable, are unlikely to be water conduits. However, the magnetic patterns follow the overall structural grain that was created by faults associated with the formation of Death Valley and the flanking mountain ranges. It is likely that faults produce barriers and conduits to groundwater flow, ultimately controlling the location of springs. As pointed out by Blakely and others (2000), the correlation of spring alignments and linear magnetic anomalies is strong in the Death Valley region. Although the faults in the Stirling Quartzite are shown by our results to have no significant magnetic expression, the faults produce block structures containing magnetic beds that are ultimately responsible for the linear anomalies. In this way, patterns of spring occurrence and linear aeromagnetic anomalies may both reflect the regional geologic structure.

REFERENCES

Blakely, R. J., Langenheim, V. E., Ponce, D. A., and Dixon, G. L., 2000, Aeromagnetic survey of the Amargosa Desert, Nevada and California: A tool for understanding near-surface geology and hydrology: U. S. Geological Survey Open-File Report 00-188, 26 p.

Jennings, C. W., 1977, Geologic Map of California: California Division of Mines and Geology, Geologic Data Map No. 2, scale 1:750,000.

Stewart, J. H., and Carlson, J. E., 1978, Geologic map of Nevada: U. S. Geological Survey, scale 1:500,000.

Wright, L. A., and Troxel, B. W., 1989a, Geologic map of the central and northern Funeral Mountains and adjacent areas, Death Valley region, southern California: U. S. Geological Survey Open-File Report 89-348, map scale 1:48,000, 7 p. pamphlet.

Wright, L. A., and Troxel, B. W., 1989b, Geologic sections to accompany geologic map of the central and northern Funeral Mountains and adjacent areas, Death Valley region, southern California, U. S. Geological Survey Open-File Report 89-647.

Table 1. Magnetic susceptibility readings in the Funeral Mountains, California and Nevada

Site #	Latitude	Longitude	1	2	3	4	5	6	7	8	9	10	11	Lithology
01SQ001	36 38.677	116 43.214	0.03	0.06	0.06	0.06								Fine-grained quartzite
01SQ002	36 38.481	116 44.041	0.20	0.25	0.07	0.83	9.85	2.40	4.39	0.33	1.14	0.27		Fine-grained quartzite
01SQ003	36 38.241	116 44.900	0.35	0.26	0.41	0.28	0.40	0.06	0.16	0.01				Very fine-grained quartzite
01SQ004	36 38.164	116 45.029	0.11	0.08	0.14	0.10	0.11	0.08	0.10	0.11	0.25	0.01		Medium-grained quartzite
01SQ005	36 38.225	116 45.075	0.13	0.11	0.17	0.17	0.14	0.14	0.08	0.08	0.18	0.08	0.06	Limestone
01SQ006	36 38.294	116 45.238	0.35	0.09	0.11	0.11	0.10	0.10	0.10	0.19				Fine-grained quartzite
01SQ007	36 38.337	116 45.305	0.07	0.05	0.13	0.07	0.05	0.06	0.09	0.05	0.09	0.04		Fine-grained quartzite
01SQ008	36 38.362	116 45.500	0.11	0.10	0.16	0.13	0.08	0.06	0.10	0.15	0.09	0.14		Very fine-grained quartzite
01SQ009	36 38.245	116 46.067	0.56	0.21	1.97	0.71	0.06	4.57	0.19	3.18	0.19	1.97		Quartzite
01SQ010	36 38.205	116 46.243	0.22	0.16	0.11	0.07	0.15	0.33	75.1	0.06	17.7	3.88	0.15	Quartzite
01SQ011	36 38.234	116 46.952	0.07	0.06	0.06	0.04	0.06	0.05						Quartzite
01SQ012	36 38.007	116 46.843	0.06	0.08	0.17	0.15	0.04	0.10	0.28	0.08	0.11	0.05		Fine-grained quartzite
01SQ013	36 38.093	116 46.637	0.14	0.10	1.34	0.62	0.24	0.36	0.79	0.50				Fine-grained quartzite
01SQ014	36 38.742	116 43.883	0.21	0.11	0.07	3.17	0.27	26.5						Fine-grained quartzite
01SQ015	36 38.582	116 44.013	0.01	0.02	0.02	0.07	0.12	1.77	0.06					Fine-grained quartzite
01SQ016	36 38.623	116 44.043	0.07	0.13	0.08	0.03	0.02	0.09	0.03					Fine-grained quartzite
01SQ017	36 38.774	116 44.277	8.90	1.81	16.6	24.0	5.99	28.7	4.45	48.1	3.18	1.79	1.35	Fine-grained quartzite
01SQ018	36 38.779	116 44.397	0.08	0.11	0.13	0.13	0.08	0.10						Fine-grained quartzite
01SQ019	36 38.809	116 44.630	1.02	6.22	0.72	0.08	0.15	0.55	0.25					Fine-grained quartzite
01SQ020	36 38.847	116 44.666	33.0	0.61	9.95	20.8	0.30							Slate
01SQ021	36 38.475	116 44.471	26.9	7.28	0.33	4.02	2.24							Fine-grained quartzite and schist
01SQ022	36 38.490	116 44.448	8.15	10.3	24.1	7.75								Fine-grained quartzite and schist
01SQ023	36 38.600	116 44.379	0.19	1.04	1.45	0.10	0.28	1.04	2.56	0.57	2.62	0.11		Quartzite

Table 1. cont.

01SQ024	36 38.576	116 44.372	0.44	0.23	0.35	0.54				Fine-grained quartzite
01SQ025	36 38.674	116 44.354	0.56	3.22	7.30	3.57	1.17	16.3	28.1	Schist
01SQ026	36 38.709	116 44.366	15.8	27.2	16.4	25.3	10.6	7.66	13.5	Schist
01SQ027	36 38.986	116 44.175	15.4							Schist
01SQ028	36 38.341	116 44.104	25.5							Schist
01SQ029	36 38.035	116 45.353	2.52							Schist
01SQ030	36 37.937	116 45.414	0.02	0.24	0.06	0.03				Fine-grained quartzite
01SQ031a	36 38.044	116 44.226	0.07	0.66	58.0	9.21				Fine-grained quartzite and schist
01SQ031b	36 38.260	116 45.095	1.06	0.53	0.32	0.58				Schist
01SQ032	36 38.340	116 45.015	150	160						Schist
01SQ033	36 38.514	116 44.909	35.0	22.0						Schist
01SQ034	36 38.521	116 44.881	20.0	30.0						Metashale

Notes: Susceptibility readings in units of 0.001 SI. See Figure 2 for sites keyed to last two digits of Site #.